Representing the impact of *Rhizophora* mangroves on flow in a hydrodynamic model (COAWST_rh v1.0): the importance of three-dimensional root system structures

Masaya Yoshikai[1,2], Takashi Nakamura[1], Eugene C. Herrera[3], Rempei Suwa[4], Rene Rollon[5], Raghab Ray[6], Keita Furukawa[7], and Kazuo Nadaoka[1]

[1]School of Environment and Society, Tokyo Institute of Technology, Tokyo 152-8552, Japan
[2]Coastal Marine Group, School of Science, University of Waikato, Private Bag 3105, Hamilton, 3240, New Zealand
[3]Institute of Civil Engineering, University of the Philippines, Diliman, Quezon City 1101, Philippines
[4]Forestry Division, Japan International Research Center for Agricultural Sciences (JIRCAS), Ibaraki 305-8686, Japan
[5]Institute of Environmental Science & Meteorology, College of Science, University of the Philippines, Diliman, Quezon City, 1001, Philippines
[6]Atmosphere and Ocean Research Institute, The University of Tokyo, Chiba, 277-8564, Japan
[7]NPO Association for Shore Environment Creation, Kanagawa, 220-0023, Japan

Correspondence to: Masaya Yoshikai (yoshikai.masaya@gmail.com)

Abstract. Coastal wetland vegetations are known to promote sedimentation by modulating flow and sediment transport, which may counteract the threats of sea-level rise. Hydrodynamic models incorporating the impact of vegetation on flow could serve a fundamental role in understanding the sedimentary processes in coastal wetlands in which vegetation is commonly approximated as an array of vertical cylinders or represented by increased bed roughness. However, this simple approximation may not be valid in the case of *Rhizophora* mangroves that have complicated three-dimensional root structures. To better understand the sedimentary processes in mangrove forests, here, we present a new model to represent the impacts of *Rhizophora* mangroves on flow in hydrodynamic models. The model explicitly accounts for the effects of the three-dimensional root structures on mean flow and turbulence, as well as the effects of two different length scales of vegetation-generated turbulence characterized by stem diameter and root diameter. The model employs an empirical model for the *Rhizophora* root structures that can be applied using basic vegetation parameters (mean stem diameter and tree density), without rigorous measurements of the root structures. We showed that compared to the conventional approximation using an array of cylinders or increased bed roughness, the new model significantly improves the predictability of velocity, turbulent kinetic energy, and bed shear stress measured in a model and a real *Rhizophora* mangrove forest. Overall, the presented model offers a realistic but feasible framework for simulating flows in *Rhizophora* mangrove forests, which may advance our understanding of the sedimentary processes within these vital ecosystems.

1 Introduction

Mangroves are one of the coastal wetland ecosystems that grow in intertidal areas in tropical and subtropical regions (Hamilton and Casey, 2016). They have characteristic aboveground root systems of which morphological structures considerably vary among genera, such as pneumatophores or "pencil roots" of *Avicennia* and *Sonneratia* genera, and prop roots of *Rhizophora* genus (Krauss et al., 2014). Especially due to the presence of aboveground root systems, mangroves exert drag against water flow that slows down flow velocity and creates conditions preferable for the deposition and retention of tidally and fluvially transported sediments (Furukawa et al., 1997; Krauss et al., 2003; Horstman et al., 2015; Chen et al., 2016, 2018; Willemsen et al., 2016; Best et al., 2022) similar to other wetland vegetation habitats such as salt marshes (Temmerman et al., 2005; Bouma et al., 2007; Mudd et al., 2010; Weisscher et al., 2022). The vegetation-flow-sediment interaction is considered a major driving factor of the long-term geomorphic evolution of wetland vegetation habitats (Mariotti and Fagherazzi, 2010; Mariotti and Canestrelli, 2017; Brückner et al., 2019; Kalra et al., 2022; Willemsen et al., 2022) that enabled them to counteract the threats due to sea-level rise (Fagherazzi et al., 2012, 2020; Lovelock et al., 2015; Kirwan et al., 2016). In order to effectively manage and conserve mangrove forests, a better understanding of the sedimentary processes in mangrove forests such as transport, deposition, and retention, which are predominantly governed by hydrodynamics, as well as long-term geomorphic evolution, is thus urgently needed.

Hydrodynamic models that simulate flow and sediment transport processes including deposition and retention could be a key tool to evaluate these sedimentary processes (e.g., Lokhorst et al., 2018), where the representation of vegetation drag is essentially important (Temmerman et al., 2005; Nardin et al., 2016). Several modeling studies have shown that depending on the magnitude of vegetation drag, the resulting geomorphic evolution can vary dramatically, hence the ecosystems' fate in response to sea-level rise (Boechat Albernaz et al., 2020; Xie et al., 2020). The vegetation drag in salt marshes and seagrass beds is commonly represented in hydrodynamic models by an array of vertical cylinders (cylinder drag model; Ashall et al., 2016; Zhu et al., 2020), the drag effect of which has been well documented in both for emergent and submerged cases by a number of studies (e.g., Nepf, 1999, 2012). Although fewer compared to studies on salt marshes, some modeling studies have evaluated flow and sediment transport processes in mangrove forests (van Maanen et al., 2015; Bryan et al., 2017; Rodríguez et al., 2017; Xie et al., 2020). However, most of them are limited to *Avicennia* or *Sonneratia*-dominated mangrove forests whose aboveground roots (pencil roots) are geometrically simple and resemble that of a cylinder array.

In contrast, the root system of *Rhizophora* genus (prop root system) has three-dimensionally complicated structures that may not be simply approximated by the array of vertical cylinders. Consequently, the representation of drag by *Rhizophora* mangroves in hydrodynamic models remains to be established despite the worldwide occurrences of this mangrove genus (Friess et al., 2019). This knowledge gap can be seen in the studies that have approximated the drag by *Rhizophora* mangroves with arbitrarily increased bed roughness (Zhang et al., 2012) or cylinder arrays with arbitrary cylinder density (Xie et al., 2020) without much theoretical and experimental support (reviewed in Le Minor et al., 2021). One exception is a modeling study by Horstman et al. (2015) that approximated the root structures of *Rhizophora* mangroves using a cylinder array with vertically

variable cylinder densities. However, their method requires an exhausting field survey of the root structures as a requirement for proper model application, which may not be feasible for a forest-scale simulation.

65   In addition to flow velocity, vegetation affects turbulence (Nepf, 2012; Xu and Nepf, 2020), which is also relevant to the transport of substances (e.g., sediment and solutes) through turbulent diffusion (Tanino and Nepf, 2008; Xu and Nepf, 2021). While several hydrodynamic models can account for the vegetation-generated turbulence for the turbulence closure (e.g., Temmerman et al., 2005, Marsooli et al., 2016), so far, no model has been established to predict the turbulence structures in *Rhizophora* mangrove forests. A rigorous, but feasible representation of the impact of *Rhizophora* mangroves on flow velocity

70   and turbulence in a hydrodynamic model is thus needed for a better understanding of sedimentary processes in *Rhizophora* mangrove forests.

Recently, insights on flow in *Rhizophora* mangrove forests have been increasing from laboratory- and field-based studies (e.g., Zhang et al., 2015; Maza et al., 2017; Shan et al., 2019; Yoshikai et al., 2022a). The availability of these studies allows us to formulate and test the representation of the impacts of *Rhizophora* mangroves on flow in hydrodynamic models. Insights

75   on root structures have also been increasing from studies that have measured root structures in relation to tree size (Ohira et al., 2013; Yoshikai et al., 2021; Mori et al., 2022). These studies have shown the possibility of predicting root structures from limited vegetation parameters such as stem diameter, which would make the model feasible to apply in a forest-scale simulation with complicated root structures that are challenging to quantify.

In order to contribute to accurate but feasible simulations of flow and thus sediment transport in *Rhizophora* mangrove

80   forests, here, we implement a new model to represent the impacts of *Rhizophora* mangroves in a three-dimensional hydrodynamic model–the Regional Ocean Modeling System (ROMS; Shchepetkin and McWilliams, 2005) of the model framework COAWST (Coupled Ocean–Atmosphere–Wave–Sediment Transport Modeling System; Warner et al., 2010). The impact of the vertically varying projected area of roots on flow velocity and turbulence is specifically taken into consideration by the new model. Furthermore, the new model accounts for two different length scales of turbulence generated by *Rhizophora*

85   mangroves–stem diameter and root diameter–as characterized by a flume experiment by Maza et al. (2017). We also incorporate an empirical *Rhizophora* root model proposed by Yoshikai et al. (2021) into the hydrodynamic model for a practical application to *Rhizophora* mangrove forests for which root structures are unknown. Here, we aim to examine the following: (a) how does the new representation of *Rhizophora* mangroves in the hydrodynamic model improve the predictability of flow velocity and turbulence compared to the conventional drag approximation using cylinder arrays or increased bed roughness?

90   (b) how can the new model be effectively applied for an accurate prediction of the flow in *Rhizophora* mangrove forests by incorporation of the *Rhizophora* root model?

2 Materials and Methods

2.1 Model description

A proposed framework for modeling the flow in *Rhizophora* mangrove forests is presented in Fig. 1. We used a three-dimensional hydrodynamic model, ROMS, under the model framework COAWST. The vegetation module has been added by Beudin et al. (2017) to account for the drag by vegetation, such as seagrasses and salt marshes, in the momentum equations in ROMS, where the formulations added are basically in the same form as the cylinder drag model (see Text S1). We modified the equations introduced by Beudin et al. (2017) to make them suitable for representing the impact of *Rhizophora* mangroves on flow; these equations are described below. We added a new module in COAWST–*Rhizophora* root module–that provides the vertical profile of the projected area density of root systems from stem diameter and tree density in each model grid (Fig. 1).
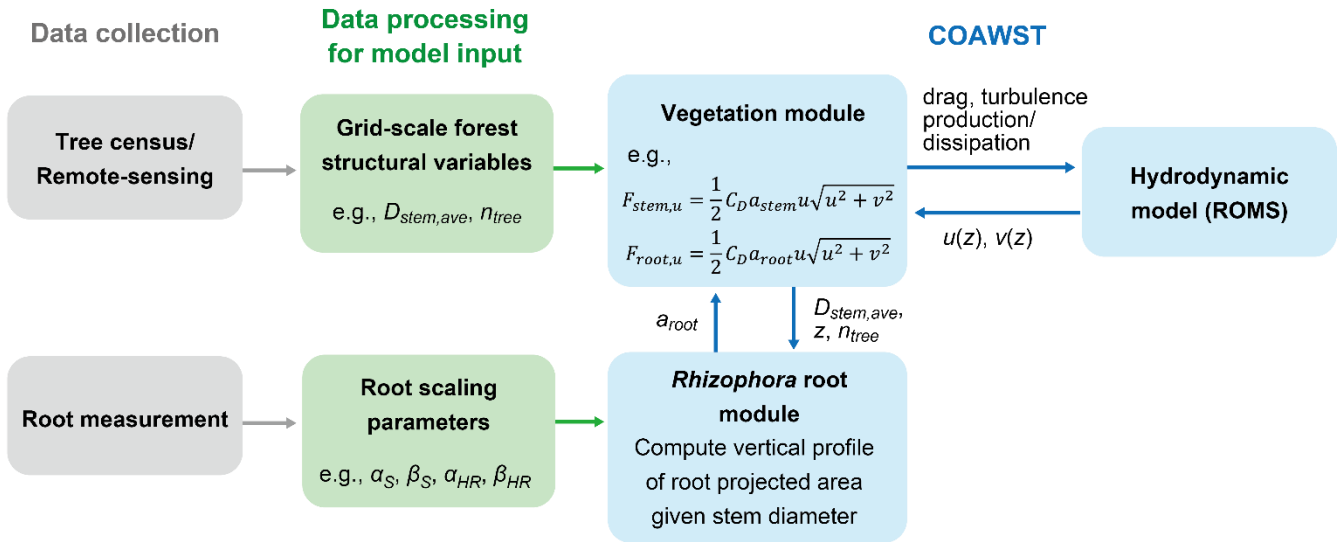
Figure 1. The proposed framework of modeling flow in *Rhizophora* mangrove forests using COAWST. $D_{stem,ave}$ and n_{tree} are the mean stem diameter and tree density, respectively, to be given in each grid, a_{stem} and a_{root} are the stem and root projected area density, where a_{stem} is a product of $D_{stem,ave}$ and n_{tree}. $F_{stem,u}$ and $F_{root,u}$ are the drag forces exerted on u-component of flow by the stem and root, respectively. See Text S3 and Table S1 for explanations of the root scaling parameters.

This manuscript basically considers velocities as temporally averaged ones unless specified. We did not consider the subgrid-scale spatial heterogeneity of velocity generated by vegetation as in other modeling studies (e.g., King et al., 2012; Marsooli et al., 2016). The Reynolds number (*Re*) defined using the root diameter as length-scale suggested fully turbulent

structures of root-generated wakes ($Re > 120$; Shan et al., 2019) even for weak currents (~1 cm s^{-1}) that could diminish the dependence of drag coefficient (C_D) on Re. Thus, we treat C_D as a constant as in Beudin et al. (2017). For simplicity, we present equations in the two-dimensional form on x-z plane (zero velocity in y-direction) while the equations implemented in ROMS are three-dimensional (x-y-z), where x-y represents the horizontal plane and z represents the vertical direction.

2.1.1 Drag force

In *Rhizophora* mangrove forests, the stem and roots are the main components that exert drag in tidal flows. We partition the drag by *Rhizophora* mangroves (vegetation drag) into the contributions by stems and roots and calculated it using the quadratic drag law as

$$F_{veg}(z) = F_{stem}(z) + F_{root}(z) = \frac{1}{2}C_D n_{tree} D_{stem,ave} u(z)^2 + \frac{1}{2}C_D a_{root}(z) u(z)^2 \tag{1}$$

where F_{veg} is the spatially-averaged vegetation drag (m s^{-2}), z is the height from bed (m), F_{stem} and F_{root} are the contributions by stems and roots to F_{veg}, respectively, C_D is the drag coefficient, n_{tree} is the tree density (m^{-2}), $D_{stem,ave}$ is the mean stem diameter (m), a_{root} is the spatially-averaged projected area density of roots (m^{-1}), and u is the flow velocity (m s^{-1}). We represented stems as cylindrical shapes with vertically uniform diameter (Maza et al., 2017) then calculated the F_{stem} using the cylinder drag model–the same equations introduced by Beudin et al. (2017) (Text S1 and Table 1). Here, we assumed the vertically constant and uniform drag coefficient (C_D) for stems and roots.

2.1.2 Turbulence

In ROMS, the generic length-scale (GLS) model is implemented as the turbulence closure, where the equations can represent several two-equation closure models such as k–ε and k–ω models by adjusting the model parameters (Umlauf and Burchard, 2003; Warner et al., 2005). In this manuscript, we present equations in the form of k–ε model for reference purposes as this is the most studied two-equation closure model for flows in vegetated areas (López and García, 2001; Katul et al., 2004; Defina and Bixio, 2005; King et al., 2012). Beudin et al. (2017) have included an additional term for wake production due to vegetation (P_w) in the equation for turbulence kinetic energy (TKE) as

$$\frac{\partial k}{\partial t} + u\frac{\partial k}{\partial x} = \frac{\partial}{\partial z}\left(\frac{v_t}{\sigma_k}\frac{\partial k}{\partial z}\right) + P_s + B + P_w - \varepsilon \tag{2}$$

where k is TKE (m^2 s^{-2}), v_t is the eddy viscosity (m^2 s^{-1}), σ_k is the turbulent Schmidt number for k (1.0), P_s, B, and P_w represent the production of k by shear, buoyancy, and wakes generated by vegetation (m^2 s^{-3}), respectively, and ε is the turbulent dissipation (m^2 s^{-3}). Similarly, they included an additional term (D_w) in the equation for ε as

$$\frac{\partial \varepsilon}{\partial t} + u\frac{\partial \varepsilon}{\partial x} = \frac{\partial}{\partial z}\left(\frac{v_t}{\sigma_\varepsilon}\frac{\partial k}{\partial z}\right) + \frac{\varepsilon}{k}(c_1 P_s + c_3 B - c_2 \varepsilon) + D_w \tag{3}$$

where σ_ε is the turbulent Schmidt number for ε (1.3), c_1 (1.44), c_2 (1.92), and c_3 are the model constants, where the value of c_3 varies depending on stratification state (Warner et al., 2005), and D_w is the dissipation rate of wakes (m^2 s^{-4}). The wake

140 production rate (P_w) is typically considered equal to the rate of work done by the flow against vegetation drag, i.e., $P_w = F_{veg}u$ (Nepf, 2012). In contrast, the turbulence dissipation rate largely depends on the turbulence length-scale in addition to the TKE, which requires a prior knowledge of the turbulence length-scale of wakes for correctly predicting the D_w (King et al., 2012; Liu et al., 2017; Li and Busari, 2019).

Previous flume studies for flow through vegetated area have shown that the stem diameter (or leaf width) is the plausible

145 turbulence length-scale of wakes (Tanino and Nepf, 2008; King et al., 2012). In the case of flow in *Rhizophora* mangrove forests, however, there are two potential length-scales–stem diameter and root diameter, which could significantly differ from each other (Maza et al., 2017). This variation makes it challenging to parameterize them into one representative length-scale of wakes (L in Eq. S6 in Text S2). To resolve this, we partitioned the P_w and D_w into the terms for wakes generated by stems and roots, respectively, as

150
$$P_w = P_{w,stem} + P_{w,root} = F_{stem}u + F_{root}u \tag{4}$$

$$D_w = D_{w,stem} + D_{w,root} = c_2\frac{P_{w,stem}}{\tau_{stem}} + c_2\frac{P_{w,root}}{\tau_{root}} \tag{5}$$

where $P_{w,stem}$ and $P_{w,root}$ (m^2 s^{-3}) are the production of k by stem- and root-generated wakes, $D_{w,stem}$ and $D_{w,root}$ (m^2 s^{-4}) are the dissipation rate of stem- and root-generated wakes, and τ_{stem} and τ_{root} (s) are the time-scale of stem- and root-generated wakes, respectively; these are given by

155
$$\tau_{stem} = \left(\frac{L_{stem}^2}{c_w^2 P_{w,stem}}\right)^{1/3} \tag{6a}$$

$$\tau_{root} = \left(\frac{L_{root}^2}{c_w^2 P_{w,root}}\right)^{1/3} \tag{6b}$$

where L_{stem} and L_{root} (m) are the length-scale of stem- and root-generated wakes, respectively, and c_w is the model constant. Here, we gave mean stem diameter ($D_{stem,ave}$) and root diameter ($D_{root,ave}$) to L_{stem} and L_{root}, respectively.

We considered c_w in Eq. (6) as a calibration parameter whereas Beudin et al. (2017) gave a value of 0.09. Tanino and

160 Nepf (2008) predicted the TKE for a flow through array of emergent cylinders with cylinder projected area density, a, and cylinder diameter, d, using $k = \gamma\left(\frac{1}{2}C_D ad\right)^{2/3}u^2$, where γ is the scale coefficient that needs to be empirically determined. We can relate c_w with γ as $c_w = \gamma^{-3/2}$ by applying the k–ε model to a limiting case of a steady, uniform, and neutrally-stratified flow through homogeneous emergent vegetation such that all the terms in Eqs. (2–3) except for k, ε, P_w, and D_w can be neglected (King et al., 2012; Liu et al., 2017). We adjusted the value of c_w so that the corresponding γ value falls within a reported range

165 (0.8–1.6; King et al., 2012; Xu and Nepf, 2020).

2.1.3 Root projected area density

We used the empirical *Rhizophora* root model (*Rh*-root model) developed by Yoshikai et al. (2021) as a predictor of the root projected area density (a_{root}) in Eq. (1). Based on an allometric relationships characterized by some site- and species-specific root scaling parameters (α_S, β_S, α_{HR}, β_{HR} in Eq. S7 in Text S3), the *Rh*-root model predicts the vertical profile of root projected area per vertical interval (dz; 0.05 m in this study) for a tree "i" ($A_{root,i}(z)$ (m^2)), where the subscript "i" represents the tree index, from the stem diameter of the tree "i" ($D_{stem,i}$). In short, $A_{root,i}(z)$ is expressed as $A_{root,i}(z) = f(D_{stem,i})$, where f represents a function of the *Rh*-root model (see Text S3 for the details).

The vertical profile of spatially-averaged projected area density of roots in each grid can be calculated as $a_{root}(z) = n_{tree} \sum_{i=1}^{Ntree} f(D_{stem,i})/(N_{tree}dz)$, where n_{tree} is the tree density (m^{-2}) and N_{tree} is the number of trees in each grid. While some variations in tree sizes (i.e., $D_{stem,i}$) and thereby $f(D_{stem,i})$, within a grid are expected, it would be convenient if the subgrid-scale variations can be parameterized using a grid-scale parameter for modeling purpose. In this study, we propose that the mean stem diameter ($D_{stem,ave}$) can be used for the parameterization as $\sum_{i=1}^{Ntree} f(D_{stem,i})/N_{tree} \approx f(D_{stem,ave})$, so that $a_{root} \approx n_{tree}f(D_{stem,ave})/dz$.

We investigated the above assumption using tree census data collected from three sites (Bak1, Bak2, and Fuk; see Text 4 for the site description). Using the *Rh*-root model, we computed the vertical distribution of the mean projected area of individuals in the tree census plots, $\sum_{i=1}^{Ntree} f(D_{stem,i})/N_{tree}$, and its representation using the mean stem diameter, $f(D_{stem,ave})$, and compared them (Fig. 2). This demonstrates that the use of $D_{stem,ave}$ can well represent the mean projected area density of individuals for all the three sites regardless of the differences in the forest structures (e.g., stem diameter distribution, tree density) and root scaling parameters (Table S1).
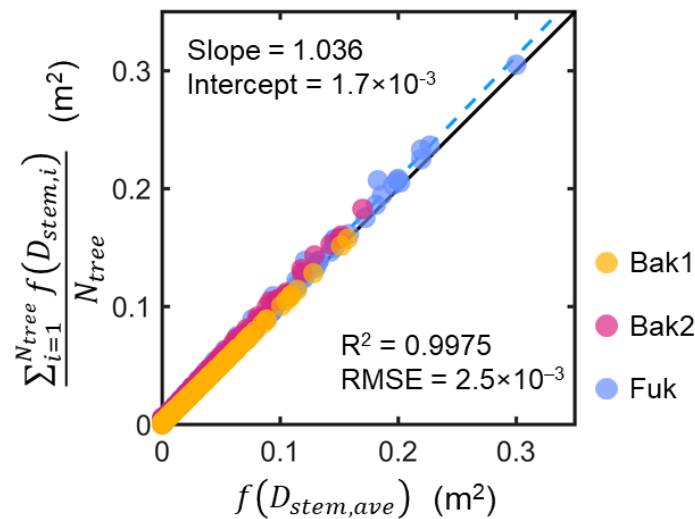
Figure 2. Comparison of the vertical profiles of mean projected area per vertical height interval (dz; 0.05 m) of individuals in tree census plots from three sites (Bak1, Bak2, and Fuk), $\sum_{i=1}^{N_{tree}} f(D_{stem,i})/N_{tree}$, and its representation using the mean stem diameter, $f(D_{stem,ave})$, where N_{tree} is the number of *Rhizophora* trees in a plot, $D_{stem,ave}$ is the mean stem diameter of *Rhizophora* trees in the plot, the subscript "i" represents the tree index, and f represents the function of the *Rhizophora* root model that gives the vertical profile of the root projected area of individuals.

2.2 Model testing

We tested the new model implemented in the COAWST against the measurements of flows in a model *Rhizophora* mangrove forest by Maza et al. (2017) and in a real planted *Rhizophora* mangrove forest by Yoshikai et al. (2022a). Text S5 provides some descriptions on the implementation of the new model to the COAWST. Both studies have provided detailed information of vegetation and hydrodynamic parameters that allow us to evaluate the model performance. Specifically, the mangrove forests in both studies have spatially uniform vegetation distribution due to the uniformly sized and evenly distributed trees (approximately, in the case of the real mangrove forest in Yoshikai et al., 2022a). Moreover, both studies have measured flow structures at a location where the flow is well developed, which eliminates the dependence of flow structures on the proximity to the forest leading edge. Given these conditions, we tested the model using a model grid assuming a schematized mangrove forest with uniform bed elevation and vegetation variables described below, and not with a grid representing the actual geometric/topographic conditions of the flume/field. Table S3 summarizes the measured hydrodynamic variables in Maza et al. (2017) and Yoshikai et al. (2022a), the variables controlled in the model, and the target variables to reproduce for each test case.

We created an orthogonal computational grid of 200 m × 200 m area with 5 m horizontal resolution for the model runs (Fig. S1). We set 15 vertical layers with approximately uniform layer thickness to be applied to the laboratory-based study. For the field-based study, the number of vertical layers was reduced to 5 because of the shallow water depths. As described above, we set the bed elevation and vegetation parameters uniform over the model domain both for the model- and real-mangrove forest test cases. To create a unidirectional flow in the model, we set the eastern and western boundaries of the model domain as closed (no water fluxes) and the northern and southern boundaries as open (Fig. S1). Then we imposed water level differences between the northern and southern boundaries to drive the flow based on the pressure gradient, where the water fluxes through the boundaries are given to equate the local pressure gradient and the drag force (bed + vegetation). The model was run with no wind conditions. When the steady state of flow was attained in the simulation, we compared the flow condition at the center of the model domain with the measurement (Fig. S1). This means that for the model application to the field mangrove forest, the actual time-series of the flow during the tidal cycle has not been reproduced; rather, steady states of flow were created for each flow measurement. Table 1 summarizes the key vegetation and hydrodynamic parameters for each test case.

We set different objectives for the model applications to the laboratory- and field-based studies, respectively. The main objective of the application to the laboratory-based study is to examine the effectiveness of the formulations for the drag and turbulence terms (Eq. (1)–(6)), which were newly implemented in the COAWST to predict the flow structures in the

220 *Rhizophora* mangrove forest, compared to the cylinder drag model. Here, we consider the vegetation frontal area density (a) as a known parameter. In contrast, the parameter a is usually unknown and needs to be predicted in the case of mangrove forests in the field. Hence, the main objective of the application to the field-based study is to examine the effectiveness of the proposed framework (Fig. 1) that includes the *Rhizophora* root model – the predictor of a – in the COAWST, compared to the drag parameterizations proposed in previous studies. Table 2 summarizes the different model configurations tested to represent

225 the impact of *Rhizophora* mangroves for the applications to the laboratory- and field-based studies. Below we describe overview of the measurements by Maza et al. (2017) and Yoshikai et al. (2022a) and the model settings.

Table 1. Vegetation and hydrodynamic parameter settings for model testing against flume experiments (Exp 1 and 2) in Maza et al. (2017) and field measurement in Yoshikai et al. (2022a). Figure S2 shows the location where the values of vegetation and hydrodynamic variables in the table were derived in Yoshikai et al. (2022a). Note that the values of vegetation and

230 hydrodynamic variables in the flume in Maza et al. (2017) were converted to the real-scale. The row for γ shows the values that best fit the measurements within the range of 0.8–1.6.

Parameter	Exp 1	Exp 2	Field
Stem diameter (D_{stem}, m)	0.2	0.2	0.066 [a]
Root diameter (D_{root}, m)	0.038	0.038	0.030 [a]
Maximum root height (HR_{max}, m)	2.01	2.01	1.10 [a]
Tree density (n_{tree}, m^{-2})	0.072	0.072	0.36
Drag coefficient (C_D)	0.8	0.8	1.0
Water depth (h, m)	3.0	1.79	0.14–0.53 [b]
Cross-sectional mean velocity (U, m s^{-1})	0.31	0.58	[c]
Scale coefficient (γ)	1.5	0.9	0.8

[a] Mean value at the measurement site.
[b] Water depth varies depending on tidal phase (see Fig. 6a, e).

[c] One of the target parameters for model prediction.

Table 2. Tested model configurations to represent the impact of *Rhizophora* mangroves against flume experiments (Exp1 and 2) in Maza et al. (2017) and field measurement in Yoshikai et al. (2022a). n_{tree}: tree density; n_v: cylinder density; $D_{stem,ave}$: mean stem diameter; b_v: cylinder density; a_{root}: root projected area density; $D_{root,ave}$: mean root diameter; z_0: bed roughness length; N_{layer}: number of vertical layers of model grid.

Test case	Model configuration	Parameter settings					
		n_{tree} or n_v (m^{-2})	$D_{stem,ave}$ or b_v (m)	a_{root} (m^{-1})	$D_{root,ave}$ (m)	z_0 (m)	N_{layer}
Flume experiment	*Rh* model	0.072 (n_{tree})	0.2 ($D_{stem,ave}$)	Measured value [a]	0.038	0.5×10^{-3} [e]	15
	Cylinder model for Exp1	1.22 (n_v)	0.038 (b_v)	-	-	0.5×10^{-3} [e]	15
	Cylinder model for Exp2	1.76 (n_v)	0.038 (b_v)	-	-	0.5×10^{-3} [e]	15
Field measurement	*Rh* model with actual a_{root}	0.36 (n_{tree})	0.066 ($D_{stem,ave}$)	Measured value [b]	0.030	0.5×10^{-3}	5
	Rh model with modeled a_{root}	0.36 (n_{tree})	0.066 ($D_{stem,ave}$)	Modeled value [c]	0.030	0.5×10^{-3}	5
	Cylinder model (sparse)	13.5 (n_v)	0.030 (b_v)	-	-	0.5×10^{-3}	5
	Cylinder model (dense)	32.3 (n_v)	0.030 (b_v)	-	-	0.5×10^{-3}	5
	Xie root model	0.36 (n_{tree})	0.066 ($D_{stem,ave}$)	Eq. (S11) [d]	0.010	0.5×10^{-3}	5
	Increased z_0	-	-	-	-	0.02	3
	No vegetation	-	-	-	-	0.5×10^{-3}	5

[a] Corresponds to the value of black markers minus $n_{tree}D_{stem,ave}$ in Fig. 3a.
[b] Corresponds to the value of black markers minus $n_{tree}D_{stem,ave}$ in Fig. 3b.
[c] Corresponds to the value of blue markers minus $n_{tree}D_{stem,ave}$ in Fig. 3b.
[d] Corresponds to the value of light green markers minus $n_{tree}D_{stem,ave}$ in Fig. 3b.
[e] Assumed value.

2.2.1 Application to a laboratory-based study

245   The model *Rhizophora* mangrove forest created in the flume by Maza et al. (2017) was $1/12^{th}$, while we ran our model in a real-scale, e.g., we converted the velocities in the flume to the real-scale by keeping the Froude number (Table 1). The real-scale vertical profile of vegetation projected area density (a) is shown in Fig. 3a. Maza et al. (2017) fabricated the root systems based on the data in Ohira et al. (2013) and distributed the model trees in-line in the flume. Maza et al. (2017) created two flow conditions by varying the water depth (h) and cross-sectional mean velocity (U) (Exp 1 and 2; Table 1) and measured the
250   vertical profiles of velocities and TKE at five lateral positions in the model forest, at which flows were fully developed (Table S3). We averaged the data taken at the five positions to estimate the spatial average of the velocity and TKE to be compared with the model output.

We imposed the real-scale vertical profile of a examined in Maza et al. (2017) (black markers in Fig. 3a) over the model domain. This means that the *Rhizophora* root module that predicts a_{root} was not applied for the simulations performed here.
255   We optimized the water levels at the boundaries to create the same flow conditions (h and U) at the center of the model domain as the ones in Exp 1 and 2, respectively.
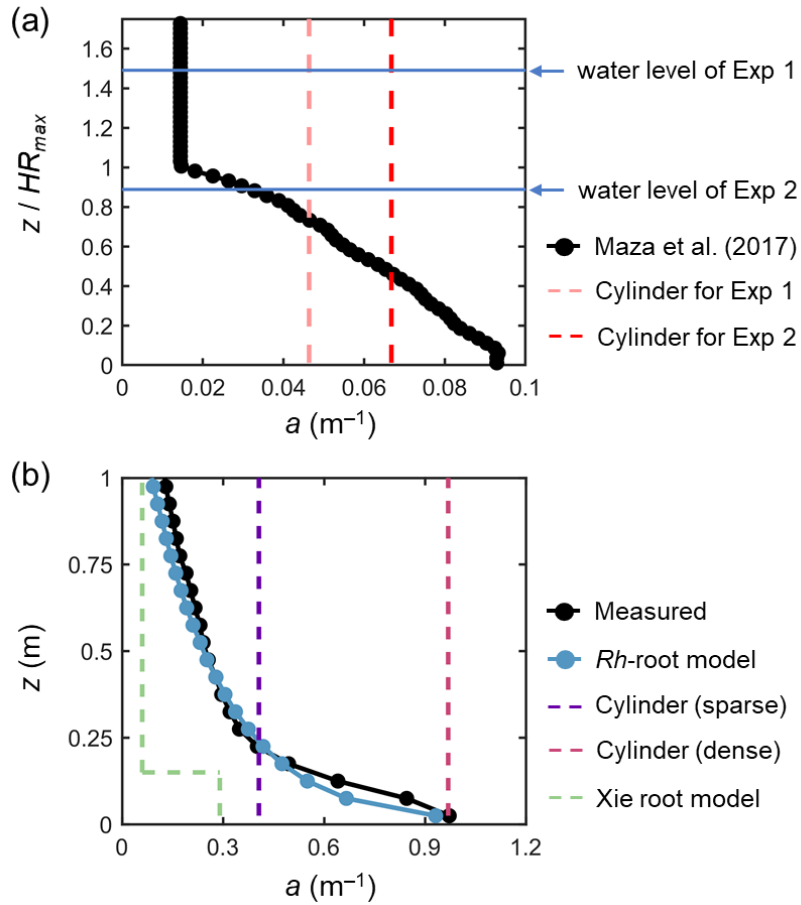
Figure 3. Vertical profiles of vegetation projected area density, a, in (a) a model *Rhizophora* mangrove forest examined by
Maza et al. (2017) and (b) a real *Rhizophora* mangrove forest examined by Yoshikai et al. (2022a), where the values were
calculated with $dz = 0.05$ m vertical interval (markers). HR_{max} is the maximum root height (2.01 m in Maza et al. (2017); Table
1). The modeled a using the *Rh*-root model in panel "b" is given by the *Rhizophora* root module using the parameters shown
in Tables 1 and S1 (for Bak2). The projected area density of cylinder arrays (in panels "a" and "b") as well as the a predicted
using the root model of Xie et al. (2020) (in panel "b"), which were used for comparison with the new model to represent the
impacts of *Rhizophora* mangroves, is also shown (dashed lines).

We used a value 0.8 for the drag coefficient (C_D) in the model (Table 1), the value of which was derived in fully developed
flows with high Reynolds numbers (> 230) by Maza et al. (2017). The value of the bottom roughness (z_0) in the flume is
unknown; hence we gave 0.5 mm to z_0, which is the value derived in the field-based study (see Section 2.2.2). Due to the
uncertainty of the bottom roughness, we did not include the modeled near-bed velocity and TKE for comparison with the
measurements, above which the velocity and TKE were insensitive to the bottom roughness. Another unknown parameter is

the scale coefficient in the turbulence closure, γ ($= c_w^{2/3}$; see Section 2.1.2). We run the model by varying γ in a reported range (0.8–1.6) with an interval 0.1 to seek a value that produced the best fit with the measurement, mostly for the TKE profile. Figure S3 provides the model sensitivity to the varying γ for the prediction of TKE profiles.

In addition to the simulation using the actual a (black markers in Fig. 3a), referred to as "*Rh* model", we tested the use of the cylinder drag model, referred to as "cylinder model" (Table 2). We defined the cylinder array for Exp 1 and 2, respectively, where the cylinder projected area density was set equal to the depth-average of the actual a for each case (dashed lines in Fig. 3a); we set the cylinder diameter equal to the root diameter of the model *Rhizophora* trees (0.038 m; Table 1). Cylinder height was set well higher than the water level to create the condition that cylinders span the entire water column – this also applies to the cylinder drag model examined in the next section.

2.2.2 Application to a field-based study

Yoshikai et al. (2022a) measured vegetation and hydrodynamic parameters at 17-year-old planted stands of *Rhizophora apiculata* in a mangrove forest locally known as Bakhwan Ecopark in Aklan, Philippines (Fig. S2). The site corresponds to Bak2 in Fig. 2. Like in the flume condition of Maza et al. (2017), approximately uniformly sized trees are evenly distributed. The measured spatially averaged vegetation projected area density (a) at the site is shown in Fig. 3b. Due to the higher complexity of the root systems and higher tree density (Table 1), the a near the bed showed almost 10 times higher value than the one in Maza et al. (2017) (Fig. 3). Yoshikai et al. (2022a) conducted hydrodynamic measurements during ebb tides on September 10 and 11, 2018 that corresponded to spring tide conditions. The measured parameters were water depth, spatially averaged velocity profile (based on measurements at four locations), water surface slope along a major flow direction, and bed shear stress (Table S3). The flow at the site is considered fully developed.

We imposed the measured water surface slope at the boundaries to drive the flow, where the water depths at the boundaries were adjusted to realize the same water depth at the center of the model domain as the measurement. We used a value 1.0 for the drag coefficient (C_D) and 0.5 mm for the bottom roughness (z_0) based on the results in Yoshikai et al. (2022a) (Table 1). As in the previous section, we changed the value of γ in a reported range (0.8–1.6) with an interval of 0.1 to seek a value that produced the best fit with the measured velocity profile. Note that the TKE profile has not been measured in the field, thus it could not be validated.

We tested seven different model configurations (Table 2): *Rh* model using the measured values for a_{root} (actual a; black markers in Fig. 3b), *Rh* model using the modeled a_{root} (blue markers in Fig. 3b), cylinder model using two different cylinder densities (sparse and dense; purple and red dashed lines in Fig. 3b), use of the other *Rhizophora* root system model used in Xie et al. (2020) as the predictor of a_{root} in Eq. (1) (Xie root model; green dashed line in Fig. 3b), increased bed roughness (z_0), and a case without imposing the vegetation drag (no vegetation). Among these, the proposed framework (Fig. 1) was used for the case *Rh* model using the modeled a_{root} (the *Rhizophora* root module provided the a_{root} in the simulation). We inputted the measured mean stem diameter ($D_{stem,ave}$) and tree density (n_{tree}) for the configuration using the *Rh* model with modeled a_{root}.

We set the sparse cylinder case based on Horstman et al. (2013) that suggested the use of vegetation geometry measured at a height of around 0.25 m for cylinder array approximation. We set the dense cylinder array to produce an equivalent resistance to Manning's coefficient of 0.14 at a water depth of 0.5 m, a value often used to represent the drag by mangroves (e.g., Zhang et al., 2012; Menéndez et al., 2020). The Xie root model predicts the root structure (a_{root}) from a given stem diameter as an array of vertical cylinders with a fixed diameter ($D_{root} = 0.01$ m) and height ($H_{root} = 0.15$ m) (see Text S6 for the model details). The vegetation frontal area (stem + root) predicted by the Xie root model using $D_{stem,ave} = 0.066$ m is shown in Fig. 3b. Here, the predicted a_{root} is used for calculating the drag by roots in Eq. (1). In addition, $D_{stem,ave} = 0.066$ m and $D_{root} = 0.01$ m were applied for L_{stem} and L_{root} in the turbulence dissipation term of Eq. (6) (Table 2). For the case of increased z_0, we reduced the number of vertical layers from 5 to 3 and set $z_0 = 0.02$ m (Table 2; see Text S7 for the details of bed shear stress calculation and the choice of the value). For the case without vegetation, z_0 is kept as 0.5×10^{-3} m, the same as the other vegetated cases. In the increased z_0 and the no vegetation cases, the bed shear stress is the main force to equate with the imposed pressure gradient.

3 Results

3.1 Comparison with a laboratory-based study

Figure 4 shows a comparison of the modeled and measured vertical profiles of velocity (u) and TKE (k) normalized by cross-sectional mean velocity (U) for Exp 1 and 2, the conditions examined by Maza et al. (2017). The profile of normalized velocity was reasonably predicted by the Rh model (Fig. 4a, c), especially at the lower part of the root system (i.e., $z/HR_{max} <$ 0.6) in Exp 1 where the velocity was greatly attenuated compared to the upper part or above the root system (Fig. 4a). The higher values of the γ lead to more homogeneous velocity profiles because of the enhanced vertical momentum exchange by the elevated TKE, while the sensitivity to the varying γ was not significant. The Rh model also predicted well the overall trend of the normalized TKE profile measured by Maza et al. (2017) for both Exp 1 and 2 by adjusting the value of γ (Fig. 4b, d). Notably, the Rh model captured well the distinct vertical variations in TKE observed in Exp 1 when $\gamma = 1.5$ (Fig. 4b), while for Exp 2, the best fit was obtained when $\gamma = 0.9$ (Fig. 4d). Overall, $\gamma = 1.2$ produced the smallest total error of Exp 1 and 2 between the model and measured values (Fig. S3). It under- and overestimated the TKE averaged over the measurement section by about 20 and 40 % for Exp 1 and 2, respectively (Fig. 4b and d), which is generally a fairly good agreement for predicting TKE.

In contrast to the Rh model, the cylinder model predicted the nearly uniform vertical profile of velocity except the region close to the bed both for Exp 1 and 2, and largely deviated from the measurements (Fig. 4a and c). The TKE predicted by the cylinder model also showed the nearly uniform vertical profile (Fig. 4b and d). While the cylinder model showed comparable TKE with the Rh model at the lower part of the root system (i.e., $z/HR_{max} < 0.4$) for both cases, it showed the significantly smaller TKE at the upper region from the Rh model and the measurement.
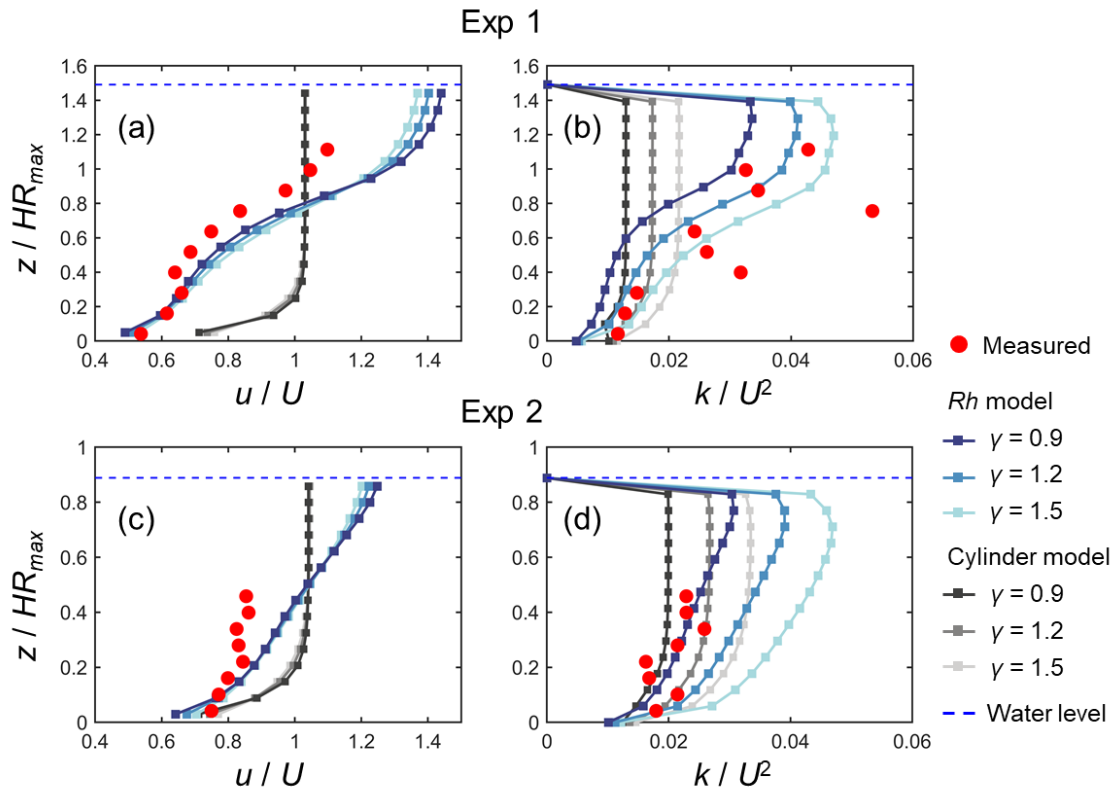
Figure 4. Comparison of the vertical profiles of (temporally and spatially averaged) velocity (u) and turbulent kinetic energy (k) normalized by the cross-sectional mean velocity (U) predicted by the COAWST with different model configurations (*Rh* model and cylinder model) and with different γ values, and measurement by Maza et al. (2017) for (a, b) Exp 1 and (c, d) Exp 2. HR_{max} is the maximum root height. Data on the measured values are provided in Table S4.

3.2 Comparison with a field-based study

Figure 5 shows the comparison of modeled velocity profiles with measurements by Yoshikai et al. (2022a) for some selected tidal phases in a *Rhizophora* mangrove forest (Bakhawan Ecopark). The *Rh* model using the measured profile of root projected area density (actual a_{root}) predicted well the overall trend of measured velocity profiles in various tidal phases (Fig. 5a). However, the model seemed to have underestimated the velocity attenuation from the surface to the bottom, which resulted in slightly higher near-bottom velocity and/or lower near-surface velocity compared to the measurement. Here, the value of γ was chosen as 0.8 from the range 0.8–1.6 (Table 2), which produced the best fit with the measured velocity profile. The *Rh* model using the modeled a_{root} provided by the *Rhizophora* root module showed a comparable performance with the use of actual a_{root} in predicting the velocity profile (Fig. 5a). However, although not significant, the use of modeled a_{root} tended to

further underestimate the velocity attenuation from the surface to the bottom due to the underestimation of a_{root} near the bed by the *Rh*-root model (Fig. 3b).

350   The cylinder model with sparse arrays showed comparable velocities with measurements near the water surface, but significantly overestimated the velocities near the bed (Fig. 5b). Alternatively, the dense arrays showed comparable velocities near the bed, but significantly underestimated the velocities near the water surface (Fig. 5c). The use of Xie root model as a predictor of a_{root} in Eq. (1) led to significant overestimation of velocities over the depths (Fig. 5d) due to the significantly underestimated vegetation projected area density (Fig. 3b). The approximation of mangrove drag in the z_0 (increased bed

355 roughness case) predicted the significant attenuation of flow velocity from the surface to the bottom due to the large bottom friction, which did not well represent the actual conditions of velocity profile in the *Rhizophora* mangrove forest (Fig. 5e). The condition without imposing vegetation drag effects led to a large overestimation of the velocities, approximately 3–4 times larger than the measurements (Fig. 5f).
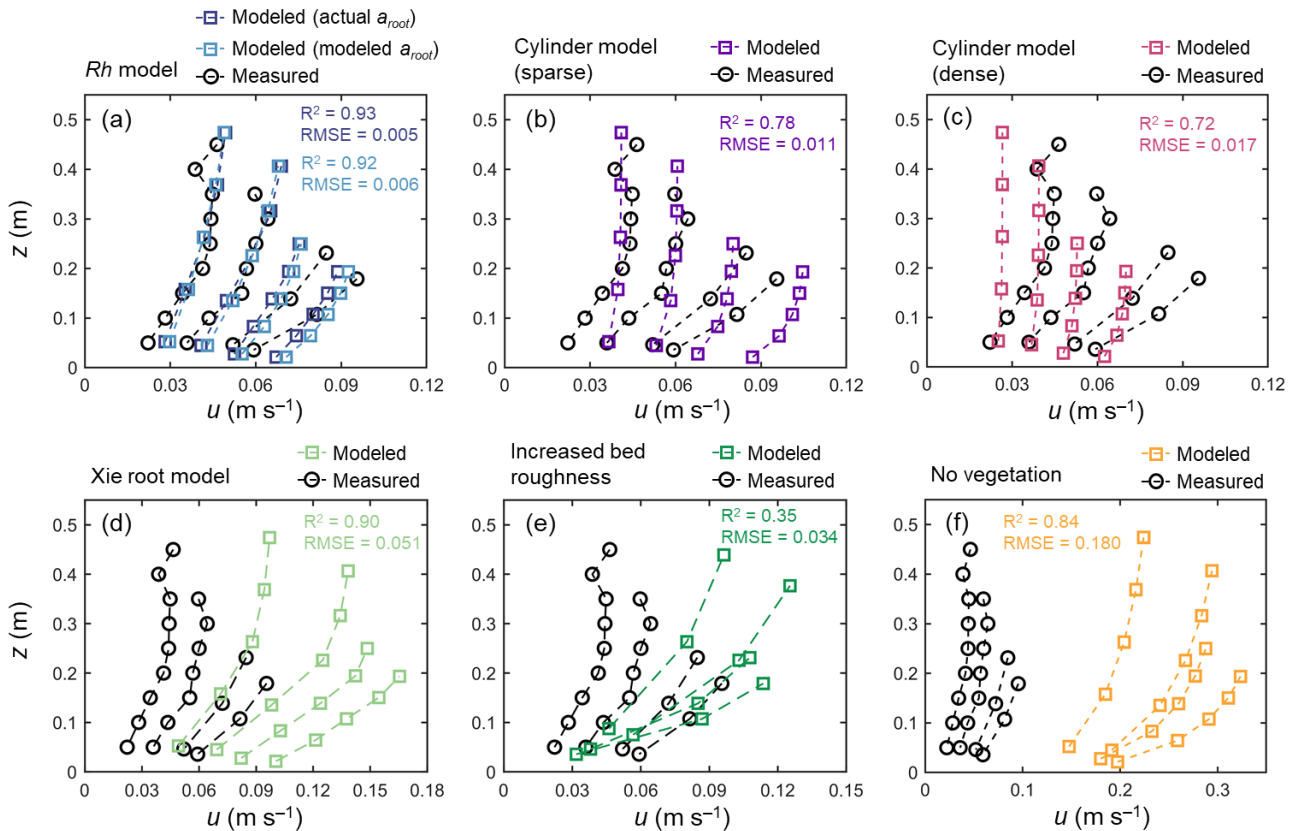
360 Figure 5. Comparison of the vertical profiles of velocity (u) predicted by the COAWST employing (a) *Rh* model using actual and modeled root projected area density profile (a_{root}), (b) cylinder model with sparse and (c) dense array, (d) Xie root model,

(e) increased bed roughness as an approximation of vegetation drag, and (f) without imposing vegetation drag (no vegetation), and measurement by Yoshikai et al. (2022a) for some selected tidal phases during the measurement period. The root mean square error (RMSE) and R^2 values of the modeled u against the measured data are also shown, for which computation of the predicted value at the height of the measurement point was obtained by the interpolation of u computed at adjacent vertical layers. Data on the measured values are provided in Table S5.

A fairly good reproduction of tidal flows by the Rh model can also be seen in the agreement with the measurement for the time-series of channel-mean velocity (U), (spatially averaged) velocity at $z = 0.05$ m (u_{bottom}), and bed shear stress (τ_{bed}) during the 2-days measurement period (Fig. 6). Note that we estimated the model prediction of velocity at $z = 0.05$ m from linear interpolation of velocities computed at adjacent vertical layers. The u_{bottom} was generally overestimated by about 15 % (Fig. 6c, g), as also seen in Fig. 5a. As a result, the τ_{bed} was overestimated by about 30 % by the model, which is still a reasonable agreement (Fig. 6d, h). As demonstrated in Fig. 5a, the Rh model employing the modeled a_{root} also showed a comparable performance for the time-series data (Fig. 6).
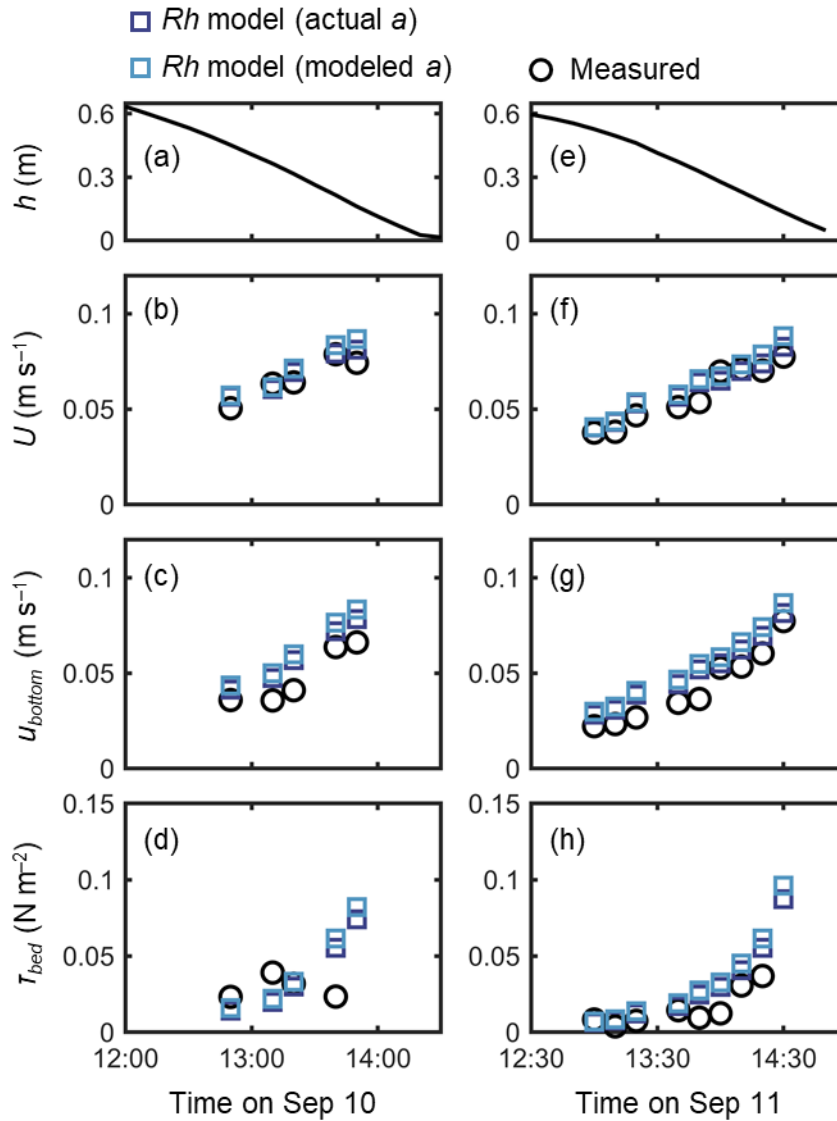
Figure 6. Time-series of (a, e) measured water depth (h), measured and predicted (b, f) cross-sectional mean velocity (U), (c, g) (spatially averaged) velocity at $z = 0.05$ m, and (d, h) bed shear stress (τ_{bed}) during the two-days measurement in Bakhawan Ecopark. The measured values are from Yoshikai et al. (2022a) and the predicted values are obtained through the COAWST employing the Rh model using actual and modeled root projected area density profile (a_{root}). Data on the measured values are provided in Table S6.

The cylinder model with sparse array led to a significant overestimation trend of the U, u_{bottom}, and τ_{bed} over the tidal phases especially when the water depth decreased (Fig. 7). The cylinder model with dense array led to the underestimation of

U most of the tidal phases but showed an agreement with the measurement for u_{bottom} and τ_{bed} (Fig. 7). The use of Xie root model resulted in consistently higher U, u_{bottom}, and τ_{bed} compared to the measured values (Fig. 8), similar to the trend seen in Fig. 5d. Although the case using the increased z_0 showed a large overestimation of flow velocities as much as the case using

385 the Xie root model when the water depth is relatively high (e.g., $h > 0.3$ m), it approached the measured values with decreasing water depth (Fig. 8); we will discuss these contrasting results in the following section. Because the bed drag is the main force to counteract the imposed pressure gradient in the increased z_0 case, the τ_{bed} showed large overestimation over the tidal phases as expected (Fig. 8c, f). The model without imposing vegetation drag led to large overestimation of these parameters over the tidal phases (Fig. S4), similar to the result shown in Fig. 5f.
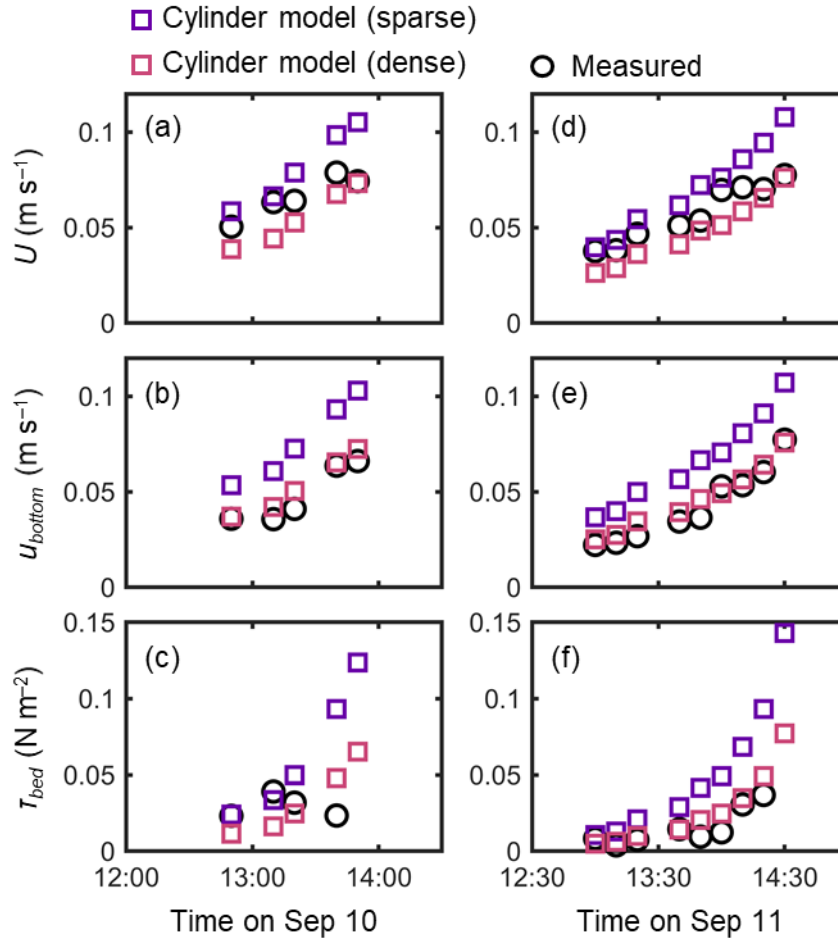
390

Figure 7. Time-series of measured and predicted (a, d) cross-sectional mean velocity (U), (b, e) (spatially averaged) velocity at $z = 0.05$ m, and (c, f) bed shear stress (τ_{bed}) during the two-days measurement in Bakhawan Ecopark. The measured values

are from Yoshikai et al. (2022a) and the predicted values are obtained through the COAWST employing the cylinder model with sparse and dense arrays.
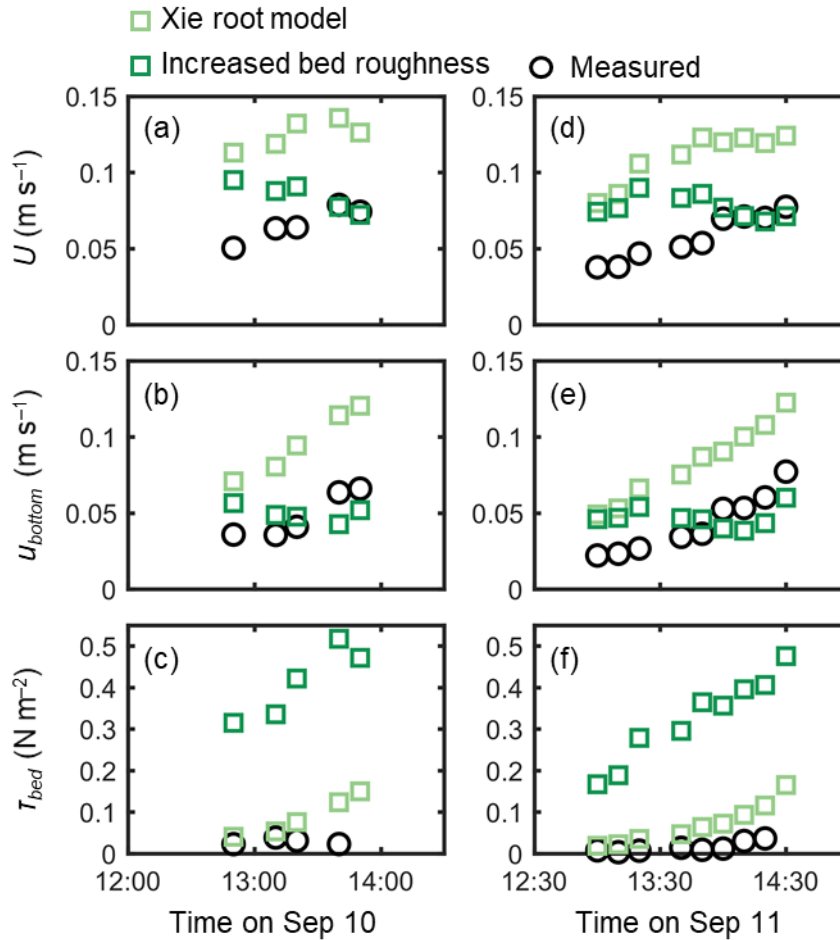
395

Figure 8. Time-series of measured and predicted (a, d) cross-sectional mean velocity (U), (b, e) (spatially averaged) velocity at $z = 0.05$ m, and (c, f) bed shear stress (τ_{bed}) during the two-days measurement in Bakhawan Ecopark. The measured values are from Yoshikai et al. (2022a) and the predicted values are obtained through the COAWST employing the Xie root model and the increased bed roughness as an approximation of drag by mangroves, respectively.

4 Discussion

4.1 Performance of the previously proposed drag parameterization

Due to the general lack of information on the vertically varying projected area of the complicated root systems, the drag by *Rhizophora* mangroves has been represented by the increased Manning's roughness coefficient values (e.g., Zhang et al., 2012) or an array of cylinders with arbitrary cylinder density (Horstman et al., 2013; Xie et al., 2020) in hydrodynamic models with 2D configuration. We evaluated these drag parameterizations using the cylinder array or increased bed roughness approximation in 3D configuration (dashed lines in Fig. 3 for the cylinder arrays). Consistent with previous studies (Liu et al., 2008; King et al., 2012), the cylinder array approximations showed the vertically uniform velocity and TKE profile except near the bed, which largely deviated from the measurements (Figs. 4 and 5). Moreover, for the tidal flows with changing water depth, the two different cylinder array configurations (sparse and dense) failed to capture the velocity changes over the tidal phases (Fig. 7) due to the inability to capture the changes in submerged vegetation projected area of *Rhizophora* mangroves.

The mangrove root model used in Xie et al. (2020) predicts the *Rhizophora* root system as an array of vertical cylinders having a fixed height and diameter. However, the root system structures of *Rhizophora* mangroves cannot be simply approximated as the array of vertical cylinders as shown in Fig. 3b. Although the shape of the velocity vertical profiles predicted using the Xie root model resembles that of observed profiles as indicated by the high R^2 value in Fig. 5d, probably due to the increased a in the root zone ($z \leq H_{root}$), the model failed to predict the absolute values as indicated by the high RMSE due to the significant underestimation of the a (Fig. 3b). Because the shape of a predicted by the Xie root model is similar to those of submerged vegetations, it is expected that the velocity inflection at the top of the root zone ($z = H_{root}$) will form as the projected area density of roots (a_{root}) further increases (e.g., King et al., 2012; Nepf 2012), which would further deviate the results from the actual velocity profiles.

Unlike the cylinder array approximations including the Xie root model where the total projected area of submerged cylinders changes with the water depth, the approximation with increased bed roughness inherently assumes the invariant area of obstructions to flows. This means that the impact of bed roughness on flow velocity becomes more significant as the water depth decreases. This effect can be seen in the prediction of cross-mean flow velocity (U) at different tidal phases where the predicted U, which was largely overestimated under the relatively high water depth ($h > 0.3$ m), approached the measured values as the water depth decreases, unlike the case using the Xie root model (Fig. 8b, e). The approximation with increased bed roughness leads to the large overestimation of τ_{bed} (Fig. 8c, f), hence making it not suitable for applications to sediment transport modeling in mangrove forests. Overall, none of the previously proposed drag parameterization captured well the flow structures in the *Rhizophora* mangrove forests examined in this study.

4.2 Performance of the new model

430   We proposed a new drag and turbulence model for flows in *Rhizophora* mangrove forests that works on the 3D hydrodynamic model, ROMS, and implemented in the COAWST. The model explicitly accounts for the vertically varying projected area of the root systems for drag force and TKE production in 3D configuration. In addition, the model accounts for the two different length-scales of wakes (roots- and stem-generated wakes) in the turbulence closure model (k–ε model in this study), an aspect none of the modeling studies has examined yet (e.g., López and García, 2001; King et al., 2012). With the

435   relatively simple modifications made to the equations introduced by Beudin et al. (2017) (Eqs. 1, 4–6), our results showed significantly improved reproducibility of ROMS for the vertical profiles of velocity and TKE, and velocity changes over the tidal phases in *Rhizophora* mangrove forests (Figs. 4, 5, and 6). The new model also reasonably predicted the bed shear stress together with these parameters (Fig. 6d and h). Although some studies have accounted for the vertically varying vegetation projected area in hydrodynamic models for salt marshes (Temmerman et al., 2005) or mangrove forests with *Rhizophora* stands

440   (Horstman et al., 2013, 2015), the efficacy of accounting for the vegetation 3D structures in the model has not been demonstrated. Overall, this is the first modeling study to introduce the realistic representation of the influences of *Rhizophora* mangrove morphological structures on the flow that was validated with existing data. The good performance of the model in both the model- and real-*Rhizophora* mangrove forests suggests the model's applicability to forests having the vegetation density a in the range 0.09–0.9 m^{-1} near the bed (Fig. 3) and an in-line tree distribution like planted mangrove forests. However,

445   the applicability to forests having $a > 0.9$ m^{-1} and/or heterogeneous tree sizes and distribution, a condition often observed in natural mangrove forests, needs further investigation in future studies.

The laboratory-based study of Maza et al. (2017) provided valuable data for evaluating the new model for TKE in a *Rhizophora* mangrove forest, which is currently unavailable from field-based studies. They observed the elevated TKE at the upper root zone and above the root zone ($z/HR_{max} > 0.5$; Fig. 4b). Maza et al. (2017) discussed the TKE production by shear

450   (P_s in Eq. 2) as one of the main reasons of the elevated TKE. However, we found that the different dominance of the root- and stem-generated wakes over the depth can explain it, such that the lower root zone dominated by root-generated wakes with length-scale set as root diameter (0.038 m; Table 2) resulted in a higher dissipation rate (Eq. 6a), thereby lower TKE; and the higher root zone dominated by stem-generated wakes with length-scale set as stem diameter (0.2 m; Table 2) resulted in a lower dissipation rate (Eq. 6b), thereby higher TKE; and the nonlinear transition between them (Fig. 4b). This result is similar

455   to the observation by Xu and Nepf (2020) that found vertically varying turbulence integral length-scale in a canopy of a salt marsh plant *Typha*. Without accounting for the two different length-scales, the model failed to reproduce the TKE profile while the velocity profile remained similar, suggesting the minor importance of shear production in reproducing the TKE (Fig. S5). The model also predicted the gradually increasing TKE upwards in the lower root zone ($z/HR_{max} < 0.5$), which is consistent with the measurement (Fig. 4b, d). While the model showed good reproducibility of the TKE profile, it should be noted that

460   different γ values produced the best fit with the measurement for Exp1 and Exp2 (Fig. 4b, d). At this moment, the exact explanation for this observation is yet to be determined, whether it can be attributed to measurement uncertainty or processes that were not represented in the model. Further research on the turbulence structures in *Rhizophora* mangrove forests is needed.

Unlike the TKE profiles predicted for the model mangrove forest, the TKE predicted for the field mangrove forest (Bakhawan Ecopark), which has much higher vegetation complexity (higher a; Fig. 3), showed nearly uniform vertical profiles (Fig. S6), results we cannot validate at this moment. Field studies on turbulence structures are likewise needed in this sense.

From the results shown, we highlighted the importance of accounting for the vertically varying projected area of the root systems with 3D configuration for capturing the flow structures (Figs. 4–8). The model predictability is therefore dependent on the root projected area, which is typically unknown and labor-intensive to measure (Yoshikai et al., 2021). For the practical use of the model, we implemented in COAWST an empirical model for the *Rhizophora* root system (*Rh*-root model; Fig. 1) with parameterization of subgrid-scale tree variations (Fig. 2) that enables the model application without rigorous measurements of root structures. The simulation for flows in Bakhawan Ecopark using the modeled a_{root} provided by the *Rhizophora* root module showed almost identical results with the one using the measured a_{root} in the field (Figs. 5 and 6). This indicates the worth of the model framework for practically and accurately predicting the flows in real *Rhizophora* mangrove forests. The grid-scale parameters required are mean stem diameter ($D_{stem,ave}$) and tree density (n_{tree}), which are basic information collected during tree census surveys (Simard et al., 2019; Suwa et al., 2021). Although the process of collecting these spatial data is out of the scope of the study, we expect that even remotely sensed data such as airborne LiDAR (Jucker et al., 2017; Dai et al., 2018) or UAV optical imagery (Otero et al., 2018), which can detect basic tree features (e.g., tree height and crown width) that have strong relationship with stem diameter (Jucker et al., 2017; Azman et al., 2021), can provide such information effectively. Obtaining the root scaling parameters requires field surveys (Fig. 1); however, these parameters can be relatively easily obtained by sampling 10–20 trees at the site (see Yoshikai et al., 2021, 2022a for the procedure). The collection of these data is far less exhaustive than extensively measuring the vertical profile of a_{root} in the area of interest as done in Horstman et al. (2015). Therefore, the model presented in this study may achieve a realistic forest-scale numerical modeling of flows in *Rhizophora* mangrove forests in the field.

4.3 Further model improvement

Due to the lack of data on sediment dynamics in *Rhizophora* mangrove forests, we did not extend the application of the presented model to sediment transport modeling in this study. For sediment transport modeling in vegetated areas, an accurate representation of vegetation impacts on both mean flow and turbulence structures that control sediment horizontal flux, retention/erosion, and turbulent mixing, is of primary importance (Nardin and Edmonds, 2014; Xu et al., 2022). Specifically, the greatly reduced near-bed velocity compared to the upper region that may significantly contribute to the sediment retention function of *Rhizophora* mangroves may be a key factor for the sediment transport modeling in this kind of forest, which was only captured by the new model (*Rh*-model in Figs. 4–5). While we expect the improved prediction of sediment transport process in *Rhizophora* mangrove forests given the improved prediction of overall flow structures using the presented new model, future studies on model application and validation with the field data on sedimentary processes are needed.

Several recent laboratory-based studies have shown that the turbulence generated by vegetation could contribute to sediment erosion, and in that case, TKE may be a better predictor of erosion rate than bed shear stress (Tinoco and Coco, 2016; Yang and Nepf, 2018; Liu et al., 2021). Currently, most numerical models evaluate sediment erosion based on bed shear stress even for the region with vegetations (e.g., Zhu et al., 2020; Breda et al., 2021; Zhang et al., 2022). Accounting for the impact of vegetation-generated turbulence on the sediment erosion in the model may be the next step to better represent the sediment transport process in *Rhizophora* mangrove forests, where the presented model has a potential to contribute to it. Yet, the insights into the effects of turbulence on sediment erosion in *Rhizophora* mangrove forests are very limited at present, necessitating further laboratory- and field-based studies.

In order to predict the long-term geomorphic evolution of mangrove forests, the interactive feedback of vegetation-flow-sediment needs to be precisely simulated (van Maanen et al., 2015; Rodríguez et al., 2017; Xie et al., 2020). This process involves long-term changes in root structure complexity in accordance with forest growth/development–a process poorly represented in previous studies in the case of *Rhizophora* mangrove forests. An advantage of the proposed model is that the root structures of *Rhizophora* mangroves are allometrically predicted in the hydrodynamic model from the basic forest structural variables–mean stem diameter and tree density, of which long-term dynamics can now be predicted using dynamic vegetation models for mangroves (e.g., Yoshikai et al., 2022b). The coupling of the hydrodynamic-sediment transport model and the dynamic vegetation model is one of the next challenges that will advance our understanding of the long-term sedimentary processes for the evaluation of the physical aspect of mangroves' ecosystem services and vulnerability.

5 Concluding remarks

This manuscript presented a new model to represent the impacts of *Rhizophora* mangroves on flow implemented in the COAWST towards a better representation of sedimentary processes in mangrove forests. We showed that compared to the conventional approximations of the impact of *Rhizophora* mangroves using cylinder array or increased bed roughness, the new model that explicitly accounts for the three-dimensional root structures, and the two potential length-scales of vegetation-generated turbulence significantly improves the prediction of velocity and TKE in *Rhizophora* mangrove forests. Specifically, the greatly attenuated near-bed velocity due to the high root density at the lower portion of the root systems, which contributes to the lowered bed shear stress relative to a given cross-sectional mean flow, is only captured by the new model. Thus, accounting for the realistic morphological structures of *Rhizophora* mangroves in the hydrodynamic model with three-dimensional configuration is important for simulating the flow in *Rhizophora* mangrove forests. While obtaining the information on the root structures in the field of model application could be challenging, the new model is now feasible in its application to the field due to the incorporation of the empirical model for *Rhizophora* root structures to the COAWST, which could achieve a more realistic forest-scale flow simulation. While future studies on field measurements and modeling are needed to extend the presented model to sediment transport modeling, owing to the significant improvement in the prediction of overall flow structures, the model developed here may serve as a fundamental tool to advance our understanding of the

sedimentary processes in *Rhizophora* mangrove forests that play a crucial role in the mangroves' ecosystem services and vulnerability.

Code and data availability

The model codes, input data, and run scripts are available at https://zenodo.org/record/7974346 (Yoshikai, 2022).

530 **Author contributions**

MY, TN, and KN designed the study and developed the model proposed in the manuscript. MY made the necessary modifications to the model code of the COAWST and performed the analyses. TN and KN contributed to result interpretation. MY wrote the manuscript, and all the authors contributed reviewing and editing.

Competing interests

535 The authors declare that they have no conflict of interests.

Acknowledgements

The authors gratefully acknowledge the Japan International Cooperation Agency (JICA) and Japan Science and Technology Agency (JST) through the Science and Technology Research Partnership for Sustainable Development Program (SATREPS) for financially supporting the project Comprehensive Assessment and Conservation of Blue Carbon Ecosystems ad their
540 Services in the Coral Triangle (BlueCARES). We thank Dr. Charissa Ferrera for providing language help.

References

Ashall, L. M., Mulligan, R. P., van Proosdij, D., and Poirier, E.: Application and validation of a three-dimensional hydrodynamic model of a macrotidal salt marsh. Coastal Engineering, 114, 35–46. https://doi.org/10.1016/j.coastaleng.2016.04.005, 2016.

545 Azman, M. S., Sharma, S., Shaharudin, M. A. M., Hamzah, M. L., Adibah, S. N., Zakaria, R. M., and MacKenzie, R. A.: Stand structure, biomass and dynamics of naturally regenerated and restored mangroves in Malaysia. Forest Ecology and Management, 482, 118852. https://doi.org/10.1016/j.foreco.2020.118852, 2021.

Best, Ü. S., van der Wegen, M., Dijkstra, J., Reyns, J., van Prooijen, B. C., and Roelvink, D.: Wave attenuation potential, sediment properties and mangrove growth dynamics data over Guyana's intertidal mudflats: assessing the potential
550 of mangrove restoration works. Earth System Science Data, 14(5), 2445–2462. https://doi.org/10.5194/essd-14-2445-2022, 2022.

Beudin, A., Kalra, T. S., Ganju, N. K., and Warner, J. C.: Development of a coupled wave-flow-vegetation interaction model. Computers & Geosciences, 100, 76–86. https://doi.org/10.1016/j.cageo.2016.12.010, 2017.

Boechat Albernaz, M., Roelofs, L., Pierik, H. J., and Kleinhans, M. G.: Natural levee evolution in vegetated fluvial-tidal environments. Earth surface processes and landforms, 45(15), 3824–3841. https://doi.org/10.1002/esp.5003, 2020.

Bouma, T. J., Van Duren, L. A., Temmerman, S., Claverie, T., Blanco-Garcia, A., Ysebaert, T., and Herman, P. M. J.: Spatial flow and sedimentation patterns within patches of epibenthic structures: Combining field, flume and modelling experiments. Continental Shelf Research, 27(8), 1020–1045. https://doi.org/10.1016/j.csr.2005.12.019, 2007.

Breda, A., Saco, P. M., Sandi, S. G., Saintilan, N., Riccardi, G., and Rodríguez, J. F.: Accretion, retreat and transgression of coastal wetlands experiencing sea-level rise. Hydrology and Earth System Sciences, 25(2), 769–786. https://doi.org/10.5194/hess-25-769-2021, 2021.

Brückner, M. Z., Schwarz, C., van Dijk, W. M., van Oorschot, M., Douma, H., and Kleinhans, M. G.: Salt marsh establishment and eco-engineering effects in dynamic estuaries determined by species growth and mortality. Journal of Geophysical Research: Earth Surface, 124(12), 2962–2986. https://doi.org/10.1029/2019JF005092, 2019.

Bryan, K. R., Nardin, W., Mullarney, J. C., and Fagherazzi, S.: The role of cross-shore tidal dynamics in controlling intertidal sediment exchange in mangroves in Cù Lao Dung, Vietnam. Continental Shelf Research, 147, 128–143. https://doi.org/10.1016/j.csr.2017.06.014, 2017.

Chen, Y., Li, Y., Cai, T., Thompson, C., and Li, Y.: A comparison of biohydrodynamic interaction within mangrove and saltmarsh boundaries. Earth Surface Processes and Landforms, 41(13), 1967–1979. https://doi.org/10.1002/esp.3964, 2016.

Chen, Y., Li, Y., Thompson, C., Wang, X., Cai, T., and Chang, Y.: Differential sediment trapping abilities of mangrove and saltmarsh vegetation in a subtropical estuary. Geomorphology, 318, 270–282. https://doi.org/10.1016/j.geomorph.2018.06.018, 2018.

Dai, W., Yang, B., Dong, Z., and Shaker, A.: A new method for 3D individual tree extraction using multispectral airborne LiDAR point clouds. ISPRS journal of photogrammetry and remote sensing, 144, 400–411. https://doi.org/10.1016/j.isprsjprs.2018.08.010, 2018.

Defina, A. and Bixio, A. C.: Mean flow and turbulence in vegetated open channel flow. Water Resources Research, 41(7). https://doi.org/10.1029/2004WR003475, 2005.

Fagherazzi, S., Kirwan, M. L., Mudd, S. M., Guntenspergen, G. R., Temmerman, S., D'Alpaos, A., van de Koppel, J., Rybczyk, J. M, Reyes, E., Craft, C., and Clough, J.: Numerical models of salt marsh evolution: Ecological, geomorphic, and climatic factors. Reviews of Geophysics, 50(1). https://doi.org/10.1029/2011RG000359, 2012.

Fagherazzi, S., Mariotti, G., Leonardi, N., Canestrelli, A., Nardin, W., and Kearney, W. S.: Salt marsh dynamics in a period of accelerated sea level rise. Journal of Geophysical Research: Earth Surface, 125, e2019JF005200. https://doi.org/10.1029/2019JF005200, 2020.

Friess, D. A., Rogers, K., Lovelock, C. E., Krauss, K. W., Hamilton, S. E., Lee, S. Y., Lucas, R., Primavera, J., Rajkaran, R., and Shi, S.: The state of the world's mangrove forests: past, present, and future. Annu. Rev. Environ. Resour, 44(1), 89–115. https://doi.org/10.1146/annurev-environ-101718-033302, 2019.

Furukawa, K., Wolanski, E., and Mueller, H.: Currents and sediment transport in mangrove forests. Estuarine, Coastal and Shelf Science, 44(3), 301–310. https://doi.org/10.1006/ecss.1996.0120, 1997.

590 Hamilton, S. E. and Casey, D.: Creation of a high spatio-temporal resolution global database of continuous mangrove forest cover for the 21st century (CGMFC-21). Global Ecology and Biogeography, 25(6), 729–738. https://doi.org/10.1111/geb.12449, 2016.

Horstman, E. M., Dohmen-Janssen, C. M., Bouma, T. J., and Hulscher, S. J.: Tidal-scale flow routing and sedimentation in mangrove forests: Combining field data and numerical modelling. Geomorphology, 228, 244–262.
595 https://doi.org/10.1016/j.geomorph.2014.08.011, 2015.

Horstman, E., Dohmen-Janssen, M., and Hulscher, S. J. M. H.: Modeling tidal dynamics in a mangrove creek catchment in Delft3D. Coastal Dynamics Arcachon, France, 833–844, 24–28 June 2013.

Jucker, T., Caspersen, J., Chave, J., Antin, C., Barbier, N., Bongers, F., Dalponte, M., van Ewijk, K. Y., Forrester, D. I., Haeni, M., Higgins, S. I., Holdaway, R. J., Iida, Y., Lorimer, C., Marshall, P. L., Momo, S., Moncrieff, G. R., Ploton, P.,
600 Poorter, L., Rahman, K. A., Schlund, M., Sonké, B., Sterck, F. J., Trugman, A. T., Usoltsev, V. A., Vanderwel, M. C., Waldner, P., Wedeux, B. M. M., Wirth, C., Wöll, H., Woods, M., Xiang, W., Zimmermann, N. E., and Coomes, D. A.: Allometric equations for integrating remote sensing imagery into forest monitoring programmes. Global change biology, 23(1), 177–190. https://doi.org/10.1111/gcb.13388, 2017.

Kalra, T. S., Ganju, N. K., Aretxabaleta, A. L., Carr, J. A., Defne, Z., and Moriarty, J. M.: Modeling marsh dynamics using a
605 3-D coupled wave-flow-sediment model. Front. Mar. Sci. 8. doi: 10.3389/fmars.2021.740921, 2022.

Katul, G. G., Mahrt, L., Poggi, D., and Sanz, C.: One-and two-equation models for canopy turbulence. Boundary-layer meteorology, 113(1), 81–109. https://doi.org/10.1023/B:BOUN.0000037333.48760.e5, 2004.

King, A. T., Tinoco, R. O., and Cowen, E. A.: A k–ε turbulence model based on the scales of vertical shear and stem wakes valid for emergent and submerged vegetated flows. Journal of Fluid Mechanics, 701, 1–39.
610 https://doi.org/10.1017/jfm.2012.113, 2012.

Kirwan, M. L., Temmerman, S., Skeehan, E. E., Guntenspergen, G. R., and Fagherazzi, S.: Overestimation of marsh vulnerability to sea level rise. Nature Climate Change, 6(3), 253–260. https://doi.org/10.1038/nclimate2909, 2016.

Krauss, K. W., Allen, J. A., and Cahoon, D. R.: Differential rates of vertical accretion and elevation change among aerial root types in Micronesian mangrove forests. Estuarine, Coastal and Shelf Science, 56(2), 251–259.
615 https://doi.org/10.1016/S0272-7714(02)00184-1, 2003.

Krauss, K. W., McKee, K. L., Lovelock, C. E., Cahoon, D. R., Saintilan, N., Reef, R., and Chen, L.: How mangrove forests adjust to rising sea level. New Phytologist, 202(1), 19–34. https://doi.org/10.1111/nph.12605, 2014.

Le Minor, M., Zimmer, M., Helfer, V., Gillis, L. G., Huhn, K.: Flow and sediment dynamics around structures in mangrove ecosystems—a modeling perspective, in: Dynamic Sedimentary Environments of Mangrove Coasts, edited by Sidik,
620 F. and Friess, D. A., Elsevier, 83–120, https://doi.org/10.1016/B978-0-12-816437-2.00012-4, 2021.

Li, C. W. and Busari, A. O.: Hybrid modeling of flows over submerged prismatic vegetation with different areal densities. Engineering Applications of Computational Fluid Mechanics, 13(1), 493–505. https://doi.org/10.1080/19942060.2019.1610501, 2019.

Liu, C., Shan, Y., and Nepf, H.: Impact of stem size on turbulence and sediment resuspension under unidirectional flow. Water Resources Research, 57(3), e2020WR028620. https://doi.org/10.1029/2020WR028620, 2021.

Liu, D., Diplas, P., Fairbanks, J. D., and Hodges, C. C.: An experimental study of flow through rigid vegetation, J. Geophys. Res., 113, F04015, doi:10.1029/2008JF001042, 2008.

Liu, Z., Chen, Y., Wu, Y., Wang, W., and Li, L.: Simulation of exchange flow between open water and floating vegetation using a modified RNG k-ε turbulence model. Environ Fluid Mech 17, 355–372. https://doi.org/10.1007/s10652-016-9489-5, 2017.

Lokhorst, I. R., Braat, L., Leuven, J. R., Baar, A. W., Van Oorschot, M., Selaković, S., and Kleinhans, M. G.: Morphological effects of vegetation on the tidal–fluvial transition in Holocene estuaries. Earth Surface Dynamics, 6(4), 883–901. https://doi.org/10.5194/esurf-6-883-2018, 2018.

López, F. and García, M. H.: Mean flow and turbulence structure of open-channel flow through non-emergent vegetation. Journal of Hydraulic Engineering, 127(5), 392–402. https://doi.org/10.1061/(ASCE)0733-9429(2001)127:5(392), 2001.

Lovelock, C. E., Cahoon, D. R., Friess, D. A., Guntenspergen, G. R., Krauss, K. W., Reef, R., Rogers, K., Saunders, M. L., Sidik, F., Swales, A., Saintilan, N., Thuyen, L. X, and Triet, T.: The vulnerability of Indo-Pacific mangrove forests to sea-level rise. Nature, 526(7574), 559–563. https://doi.org/10.1038/nature15538, 2015.

Mariotti, G. and Canestrelli, A.: Long-term morphodynamics of muddy backbarrier basins: Fill in or empty out?. Water Resources Research, 53(8), 7029–7054. https://doi.org/10.1002/2017WR020461, 2017.

Mariotti, G. and Fagherazzi, S.: A numerical model for the coupled long-term evolution of salt marshes and tidal flats. Journal of Geophysical Research: Earth Surface, 115(F1). https://doi.org/10.1029/2009JF001326, 2010.

Marsooli, R., Orton, P. M., Georgas, N., and Blumberg, A. F.: Three-dimensional hydrodynamic modeling of coastal flood mitigation by wetlands. Coastal Engineering, 111, 83–94. https://doi.org/10.1016/j.coastaleng.2016.01.012, 2016.

Maza, M., Adler, K., Ramos, D., Garcia, A. M., and Nepf, H.: Velocity and drag evolution from the leading edge of a model mangrove forest. Journal of Geophysical Research: Oceans, 122(11), 9144–9159. https://doi.org/10.1002/2017JC012945, 2017.

Menéndez, P., Losada, I. J., Torres-Ortega, S., Narayan, S., and Beck, M. W.: The global flood protection benefits of mangroves. Scientific reports, 10(1), 1–11. https://doi.org/10.1038/s41598-020-61136-6, 2020.

Mori, N., Chang, C. W., Inoue, T., Akaji, Y., Hinokidani, K., Baba, S., Takagi, M., Mori, S., Koike, H., Miyauchi, M., Suganuma, R., Sabunas, A., Miyashita, T., and Shimura, T.: Parameterization of mangrove root structure of *Rhizophora stylosa* in coastal hydrodynamic model. Frontiers in Built Environment, 7, 782219. https://doi.org/10.3389/fbuil.2021.782219, 2022.

Mudd, S. M., D'Alpaos, A., and Morris, J. T.: How does vegetation affect sedimentation on tidal marshes? Investigating particle capture and hydrodynamic controls on biologically mediated sedimentation. Journal of Geophysical Research: Earth Surface, 115(F3). https://doi.org/10.1029/2009JF001566, 2010.

Nardin, W. and Edmonds, D. A.: Optimum vegetation height and density for inorganic sedimentation in deltaic marshes. Nature Geoscience, 7(10), 722–726. https://doi.org/10.1038/ngeo2233, 2014.

Nardin, W., Edmonds, D. A., and Fagherazzi, S.: Influence of vegetation on spatial patterns of sediment deposition in deltaic islands during flood. Advances in Water Resources, 93, 236–248. https://doi.org/10.1016/j.advwatres.2016.01.001, 2016.

Nepf, H. M.: Drag, turbulence, and diffusion in flow through emergent vegetation. Water resources research, 35(2), 479–489. https://doi.org/10.1029/1998WR900069, 1999.

Nepf, H. M.: Flow and transport in regions with aquatic vegetation. Annual review of fluid mechanics, 44, 123–142. https://doi.org/10.1146/annurev-fluid-120710-101048, 2012.

Ohira, W., Honda, K., Nagai, M., and Ratanasuwan, A.: Mangrove stilt root morphology modeling for estimating hydraulic drag in tsunami inundation simulation. Trees, 27(1), 141–148. https://doi.org/10.1007/s00468-012-0782-8, 2013.

Otero, V., Van De Kerchove, R., Satyanarayana, B., Martínez-Espinosa, C., Fisol, M. A. B., Ibrahim, M. R. B., Sulong, I., Mohd-Lokman, H., Lucas, R., and Dahdouh-Guebas, F.: Managing mangrove forests from the sky: Forest inventory using field data and Unmanned Aerial Vehicle (UAV) imagery in the Matang Mangrove Forest Reserve, peninsular Malaysia. Forest Ecology and Management, 411, 35–45. https://doi.org/10.1016/j.foreco.2017.12.049, 2018.

Rodríguez, J. F., Saco, P. M., Sandi, S., Saintilan, N., and Riccardi, G.: Potential increase in coastal wetland vulnerability to sea-level rise suggested by considering hydrodynamic attenuation effects. Nature communications, 8(1), 1–12. https://doi.org/10.1038/ncomms16094, 2017.

Shan, Y., Liu, C., and Nepf, H.: Comparison of drag and velocity in model mangrove forests with random and in-line tree distributions. Journal of Hydrology, 568, 735–746. https://doi.org/10.1016/j.jhydrol.2018.10.077, 2019.

Shchepetkin, A. F. and McWilliams, J. C.: The regional oceanic modeling system (ROMS): a split-explicit, free-surface, topography-following-coordinate oceanic model. Ocean modelling, 9(4), 347–404. https://doi.org/10.1016/j.ocemod.2004.08.002, 2005.

Simard, M., Fatoyinbo, L., Smetanka, C., Rivera-Monroy, V. H., Castañeda-Moya, E., Thomas, N., and Van der Stocken, T.: Mangrove canopy height globally related to precipitation, temperature and cyclone frequency. Nature Geoscience, 12(1), 40–45. https://doi.org/10.1038/s41561-018-0279-1, 2019.

Suwa, R., Rollon, R., Sharma, S., Yoshikai, M., Albano, G. M. G., Ono, K., Adi, N. S., Ati, R. N. A., Kusumaningtyas, M. A., Kepel, T. L., Maliao, R. J., Primavera-Tirol, Y. H., Blanco, A. C., and Nadaoka, K.: Mangrove biomass estimation using canopy height and wood density in the South East and East Asian regions. Estur. Coast. Shelf S., 248, 106937, 2021.

Tanino, Y. and Nepf, H. M.: Lateral dispersion in random cylinder arrays at high Reynolds number. Journal of Fluid Mechanics, 600, 339–371. https://doi.org/10.1017/S0022112008000505, 2008.

690 Temmerman, S., Bouma, T. J., Govers, G., Wang, Z. B., De Vries, M. B., and Herman, P. M. J.: Impact of vegetation on flow routing and sedimentation patterns: Three-dimensional modeling for a tidal marsh. Journal of Geophysical Research: Earth Surface, 110(F4). https://doi.org/10.1029/2005JF000301, 2005.

Tinoco, R. O. and Coco, G.: A laboratory study on sediment resuspension within arrays of rigid cylinders. Advances in Water Resources, 92, 1–9. https://doi.org/10.1016/j.advwatres.2016.04.003, 2016.

695 Umlauf, L. and Burchard, H.: A generic length-scale equation for geophysical turbulence models. Journal of Marine Research, 61(2), 235–265. https://doi.org/10.1357/002224003322005087, 2003.

van Maanen, B., Coco, G., and Bryan, K. R.: On the ecogeomorphological feedbacks that control tidal channel network evolution in a sandy mangrove setting. Proceedings of the Royal Society A: Mathematical, Physical and Engineering Sciences, 471(2180), 20150115. https://doi.org/10.1098/rspa.2015.0115, 2015.

700 Warner, J. C., Armstrong, B., He, R., and Zambon, J. B.: Development of a coupled ocean–atmosphere–wave–sediment transport (COAWST) modeling system. Ocean modelling, 35(3), 230–244. https://doi.org/10.1016/j.ocemod.2010.07.010, 2010.

Warner, J. C., Sherwood, C. R., Arango, H. G., and Signell, R. P.: Performance of four turbulence closure models implemented using a generic length scale method. Ocean Modelling, 8(1-2), 81–113. 705 https://doi.org/10.1016/j.ocemod.2003.12.003, 2005.

Weisscher, S. A. H., Van den Hoven, K., Pierik, H. J., and Kleinhans, M.: Building and raising land: mud and vegetation effects in infilling estuaries. Journal of Geophysical Research: Earth Surface, 127(1). https://doi.org/10.1029/2021JF006298, 2022.

Willemsen, P. W. J. M., Horstman, E. M., Borsje, B. W., Friess, D. A., and Dohmen-Janssen, C. M.: Sensitivity of the sediment 710 trapping capacity of an estuarine mangrove forest. Geomorphology, 273, 189–201. https://doi.org/10.1016/j.geomorph.2016.07.038, 2016.

Willemsen, P. W. J. M., Smits, B. P., Borsje, B. W., Herman, P. M. J., Dijkstra, J. T., Bouma, T. J., and Hulscher, S. J. M. H.: Modeling decadal salt marsh development: variability of the salt marsh edge under influence of waves and sediment availability. Water resources research, 58(1), e2020WR028962. https://doi.org/10.1029/2020WR028962, 2022.

715 Xie, D., Schwarz, C., Brückner, M. Z., Kleinhans, M. G., Urrego, D. H., Zhou, Z., and Van Maanen, B.: Mangrove diversity loss under sea-level rise triggered by bio-morphodynamic feedbacks and anthropogenic pressures. Environmental Research Letters, 15(11), 114033. https://doi.org/10.1088/1748-9326/abc122, 2020.

Xu, Y., Esposito, C. R., Beltrán-Burgos, M., and Nepf, H. M.: Competing effects of vegetation density on sedimentation in deltaic marshes. Nature communications, 13(1), 1–10. https://doi.org/10.1038/s41467-022-32270-8, 2022.

720 Xu, Y. and Nepf, H.: Measured and predicted turbulent kinetic energy in flow through emergent vegetation with real plant morphology. Water Resources Research, 56(12), e2020WR027892. https://doi.org/10.1029/2020WR027892, 2020.

Xu, Y. and Nepf, H.: Suspended sediment concentration profile in a *Typha latifolia* canopy. Water Resources Research, 57(9), e2021WR029902. https://doi.org/10.1029/2021WR029902, 2021.

Yang, J. Q. and Nepf, H. M.: A turbulence-based bed-load transport model for bare and vegetated channels. Geophysical Research Letters, 45(19), 10–428. https://doi.org/10.1029/2018GL079319, 2018.

Yoshikai, M: MasayaYoshikai/COAWST_mangrove_rh: COAWST_rh (v1.0), Zenodo [code], https://zenodo.org/record/7353835#.Y4BZoZrP1D9, 2022.

Yoshikai, M., Nakamura, T., Suwa, R., Argamosa, R., Okamoto, T., Rollon, R., Basina, R., Primavera-Tirol, Y. H., Blanco, A. C., Adi, N. S., and Nadaoka, K.: Scaling relations and substrate conditions controlling the complexity of Rhizophora prop root system. Estur. Coast. Shelf S., 248, 107014, 2021.

Yoshikai, M., Nakamura, T., Bautista, D. M., Herrera, E. C., Baloloy, A., Suwa, R., Basina, R., Primavera-Tirol, Y. H., Blanco, A.C., and Nadaoka, K.: Field measurement and prediction of drag in a planted *Rhizophora* mangrove forest. Journal of Geophysical Research: Oceans, 127, e2021JC018320. https://doi.org/10.1029/2021JC018320, 2022a.

Yoshikai, M., Nakamura, T., Suwa, R., Sharma, S., Rollon, R., Yasuoka, J., Egawa, R., and Nadaoka, K.: Predicting mangrove forest dynamics across a soil salinity gradient using an individual-based vegetation model linked with plant hydraulics. Biogeosciences, 19(6), 1813–1832. https://doi.org/10.5194/bg-19-1813-2022, 2022b.

Zhang, K., Liu, H., Li, Y., Xu, H., Shen, J., Rhome, J., and Smith III, T. J.: The role of mangroves in attenuating storm surges. Estuarine, Coastal and Shelf Science, 102, 11–23. https://doi.org/10.1016/j.ecss.2012.02.021, 2012.

Zhang, X., Chua, V. P., and Cheong, H. F.: Hydrodynamics in mangrove prop roots and their physical properties. Journal of hydro-environment research, 9(2), 281–294. https://doi.org/10.1016/j.jher.2014.07.010, 2015.

Zhang, Y., Svyatsky, D., Rowland, J. C., Moulton, J. D., Cao, Z., Wolfram, P. J., Xu, C., and Pasqualini, D. (2022). Impact of coastal marsh eco-geomorphologic change on saltwater intrusion under future sea level rise. Water Resources Research, e2021WR030333. https://doi.org/10.1029/2021WR030333.

Zhu, Q., Wiberg, P. L., and Reidenbach, M. A.: Quantifying Seasonal Seagrass Effects on Flow and Sediment Dynamics in a Back-Barrier Bay. Journal of Geophysical Research: Oceans, 126(2), e2020JC016547. https://doi.org/10.1029/2020JC016547, 2021.